Electronic Supplementary Information

A highly selective "ON-OFF" probe for colorimetric and fluorometric sensing of Cu^{2+} in water

Barnali Naskar,[a] Ritwik Modak,[a] Dilip K. Maiti,[a] Antonio Bauzá,[b] Antonio Frontera,[b] Pulak Kumar Maiti,[c] Sukhendu Mandal[c] and Sanchita Goswami[*,a]

[a]*Department of Chemistry, University of Calcutta, 92, A.P.C. Road, Kolkata-700009, India.*

[b]*Departament de Quı´mica, Universitat de les IllesBalears, Crta. deValldemossa km 7.5, 07122 Palma de Mallorca, Baleares, Spain.*

[c]*Department of Microbiology, University of Calcutta, 35, Ballygunge Circular Road, Kolkata, India.*

Contents of the Supporting Information

1. Characterization, Structure and Crystallographic Data

Pages

2. Photophysical Characterization

3. Theoretical Data

4. Miscellaneous

1.Characterization, Structure and Crystallographic Data.

^{1}H and ^{13}C−NMR spectra: H_5dpm was dissolved in d_6–DMSO and recorded with TMS as internal standard on a Bruker, AV 300 Supercon Digital NMR system.

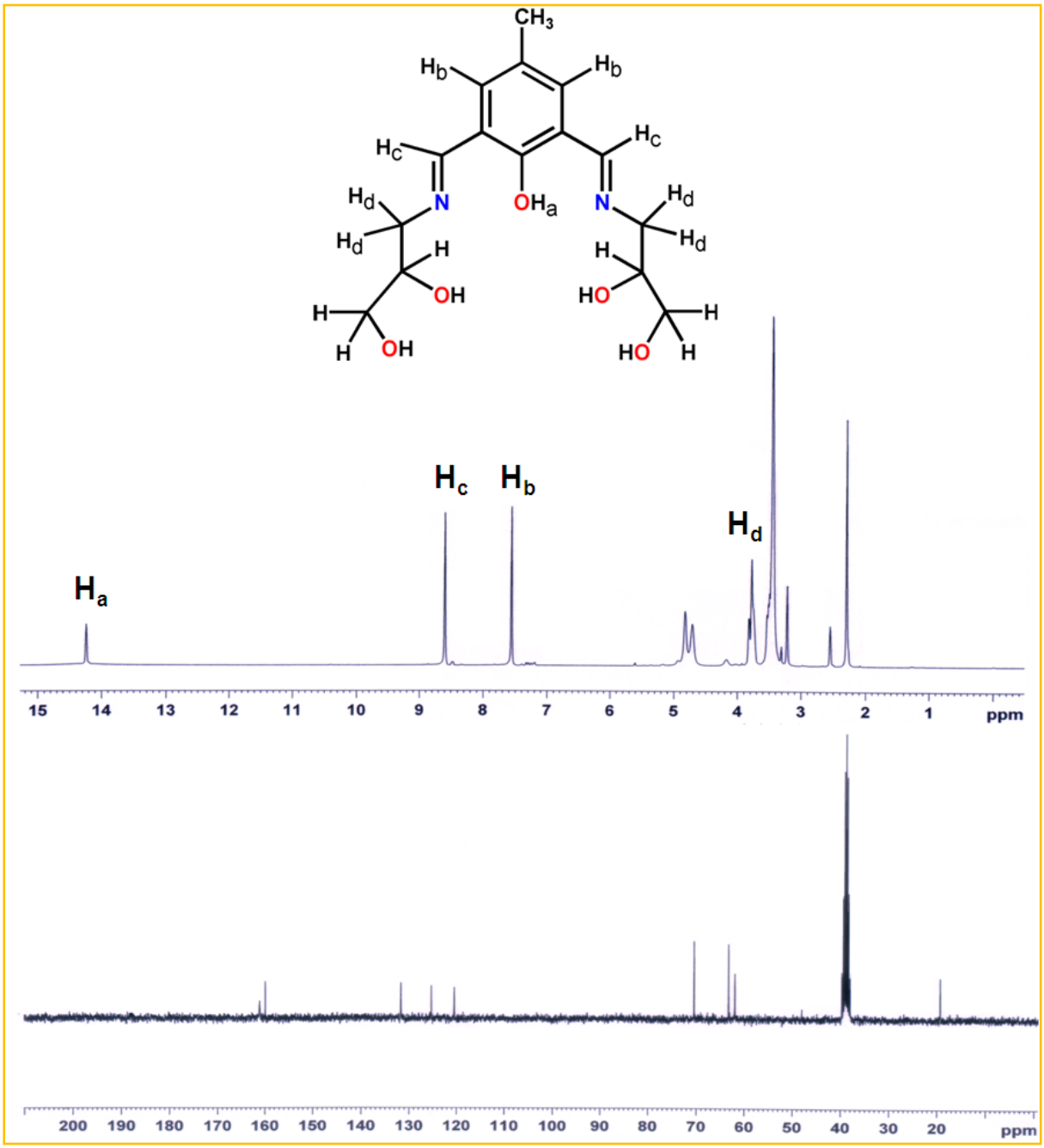

Figure S1. ^{1}H and ^{13}C−NMR spectrum of chemosensor (**H_5dpm**).

1. Characterization, Structure and Crystallographic Data.

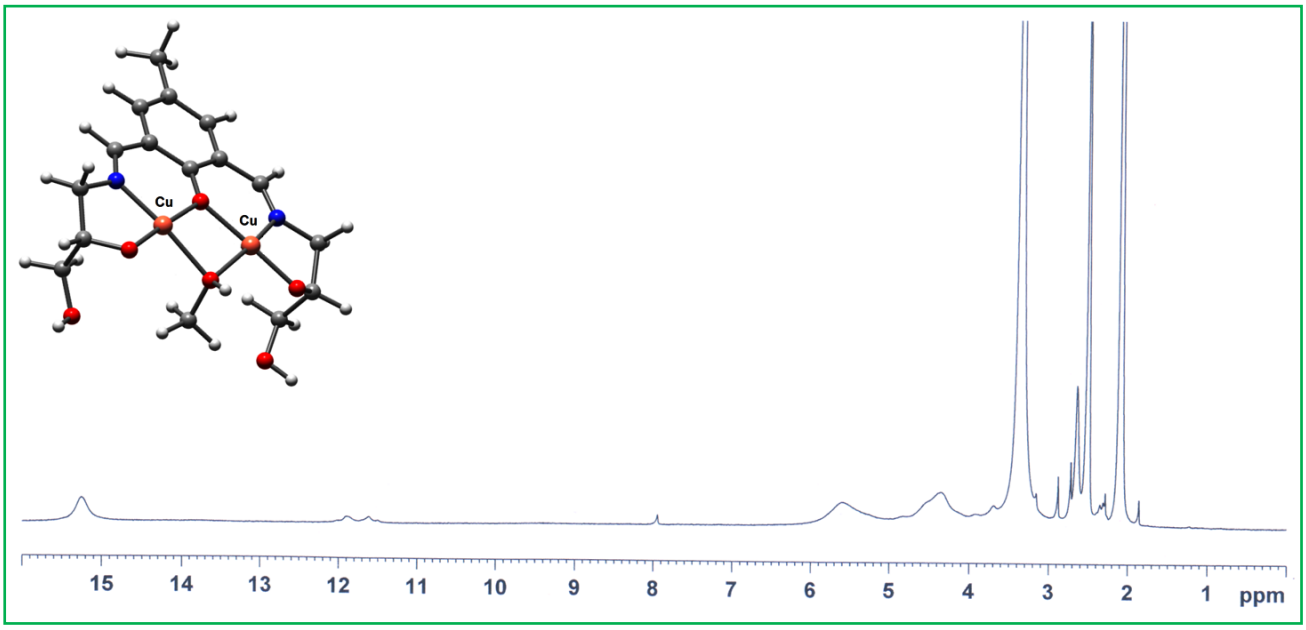

Figure S2. ^{1}H−NMR spectrum of Complex **2**.

FT–IR spectroscopy: Fourier transform infrared (FT-IR) spectra were recorded with a Perkin-Elmer RXI FT-IR spectrophotometer using the reflectance technique (4000−400 cm^{-1}). Samples were prepared as KBr disks.

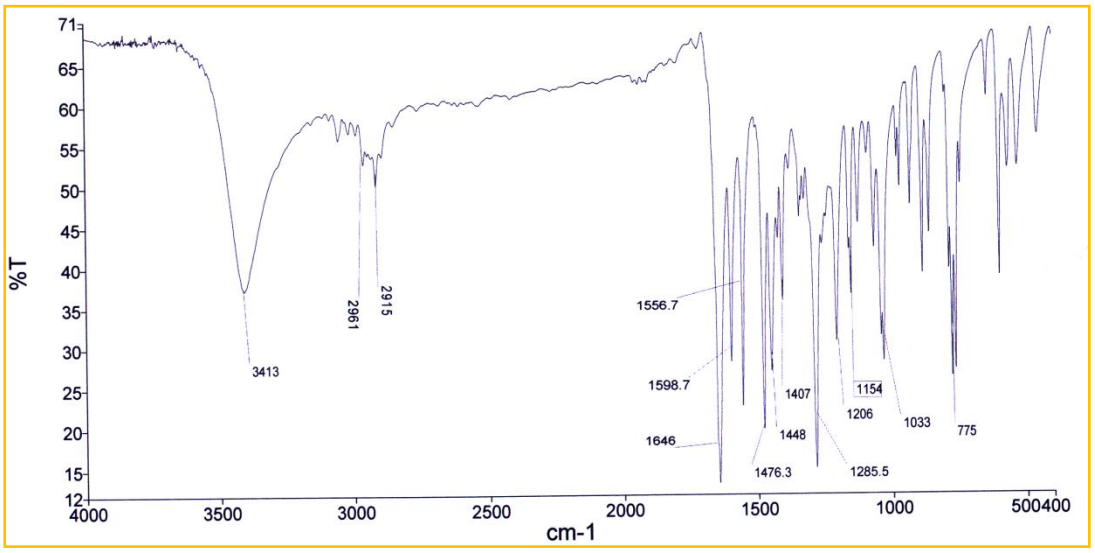

H_5dpm

1. Characterization, Structure and Crystallographic Data.

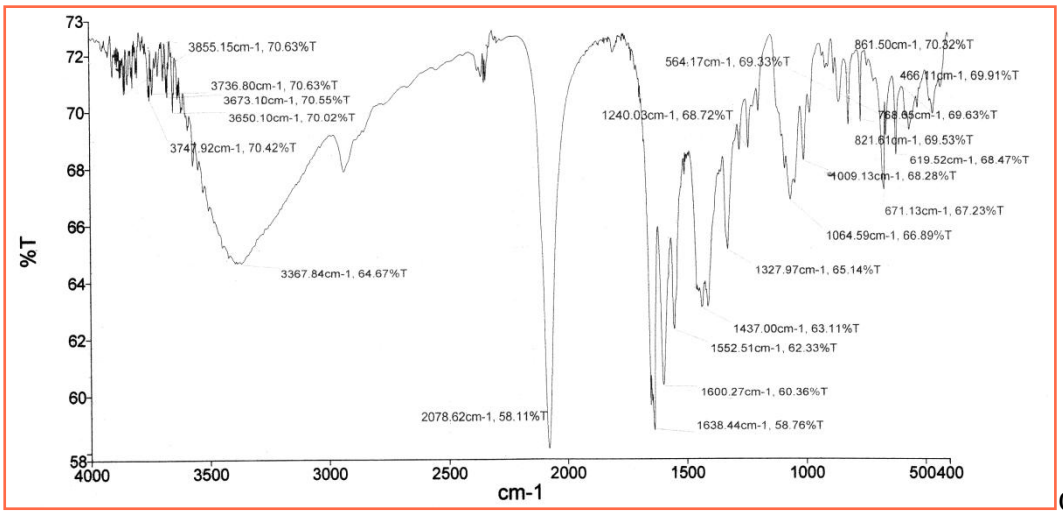

Complex **1**

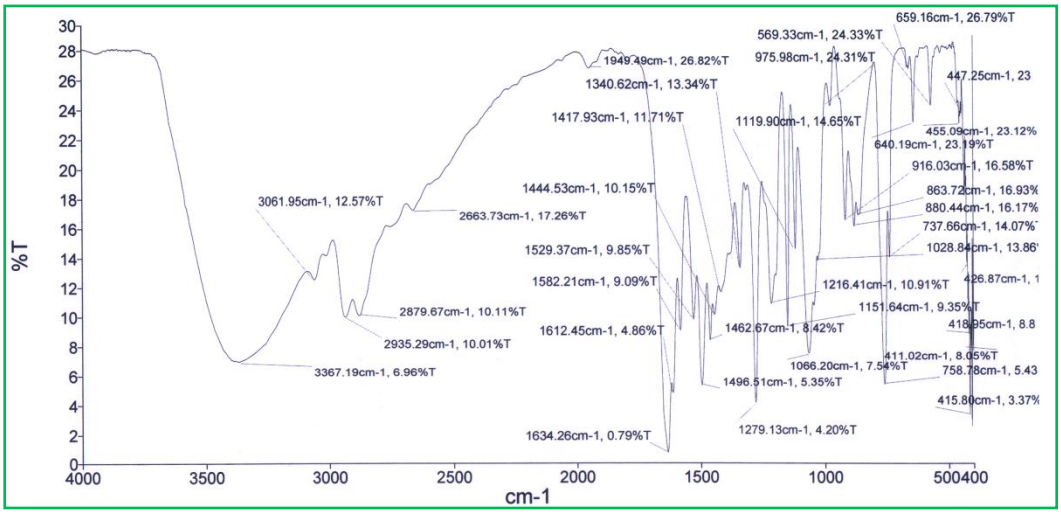

Complex **2**

Figure S3. FT-IR Spectrum of chemosensor (**H_5dpm**), complex **1** and complex **2**.

1. Characterization, Structure and Crystallographic Data.

Electrospray mass spectra (ESI-MS) were recorded on Qtof Micro YA263 mass spectrometer dissolving the samples in LC–MS quality MeOH.

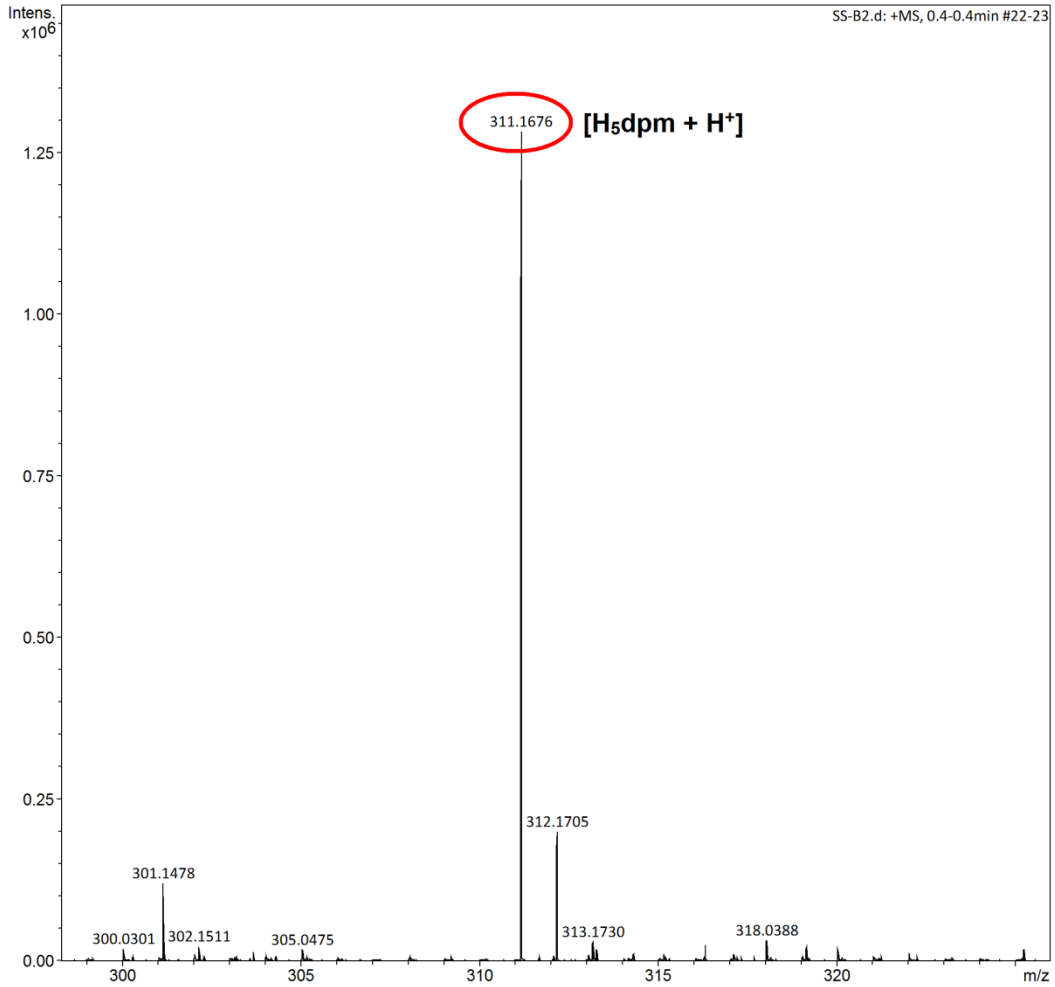

[H_5dpm]

1. Characterization, Structure and Crystallographic Data.

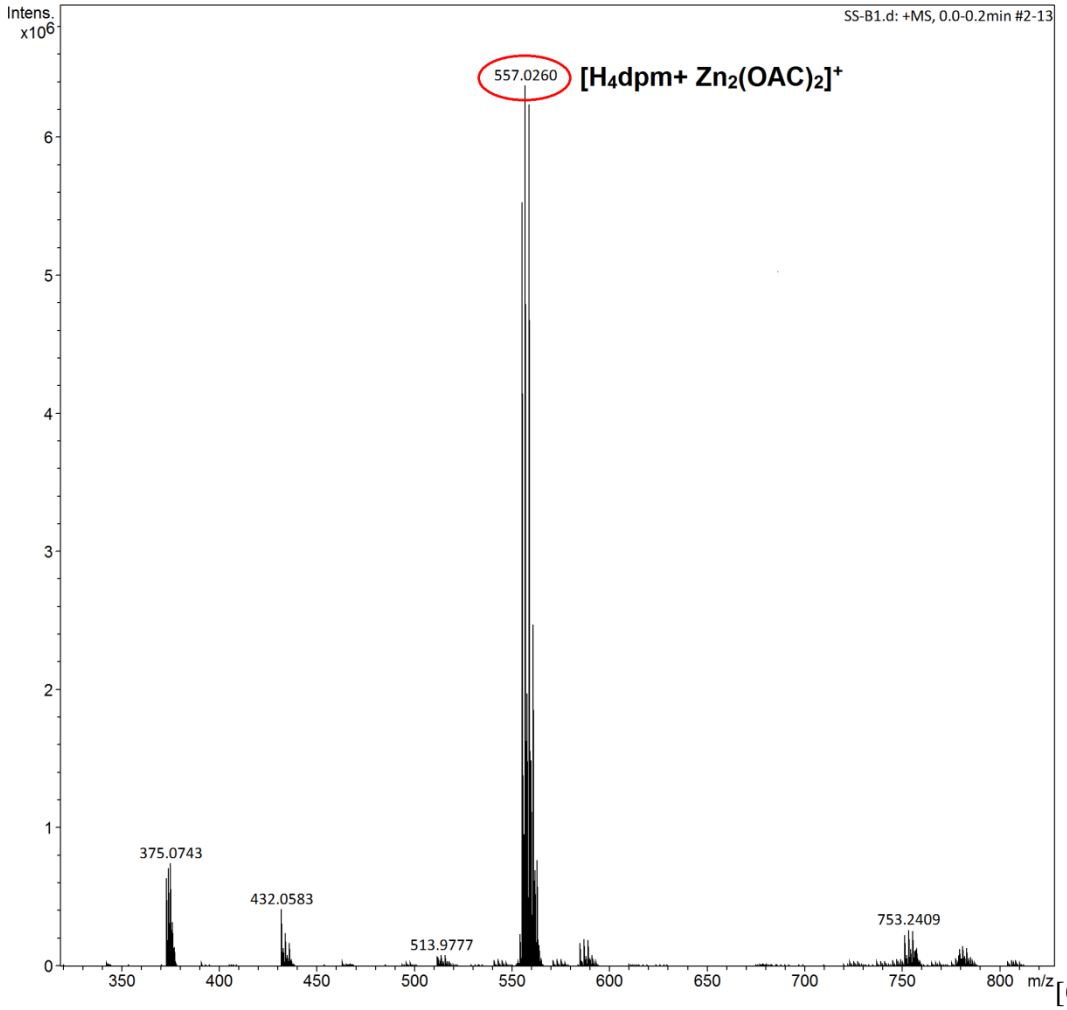

[Complex**1**]

1. Characterization, Structure and Crystallographic Data.

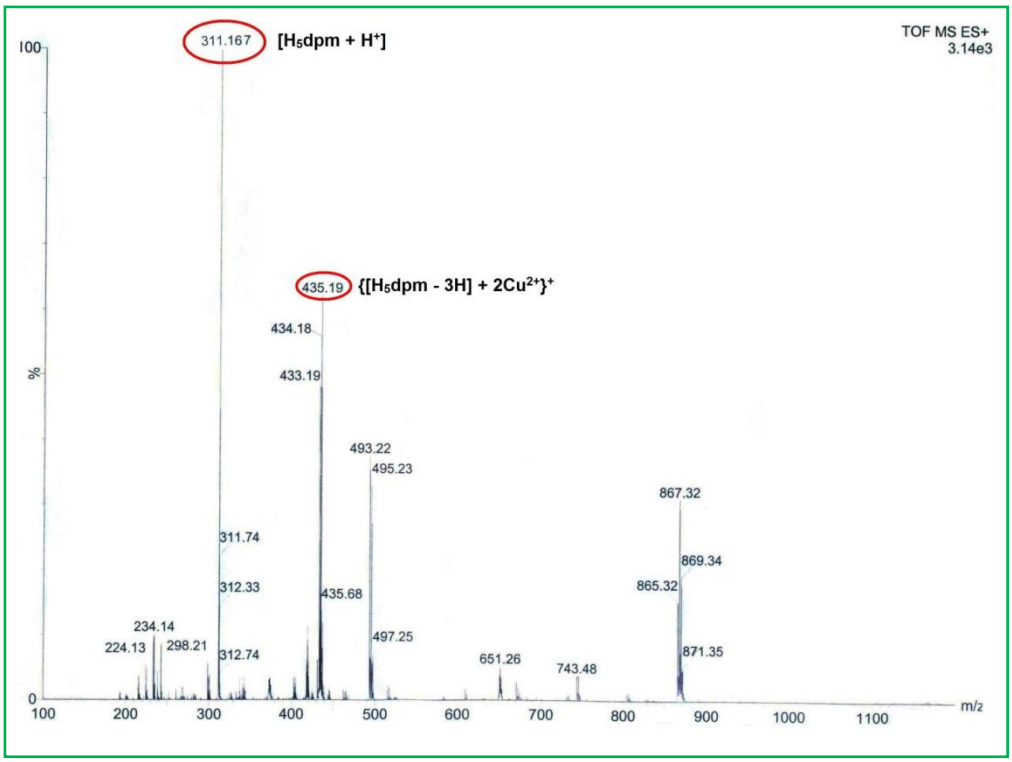

[Complex **2**]

Figure S4. ESI-MS of chemosensor (**H_5dpm**), complex **1** and complex **2**.

1. Characterization, Structure and Crystallographic Data.

Single–Crystal X–ray data collection and structure determination of Complex 1

Selected single crystals for complex **1** were mounted on Nonius APEX–II diffractometer with CCD–area detector at 296 K using graphite–monochromated Mo–Kα radiation (λ= 0.71073 Å). The structure was solved by direct methods and refined by full–matrix, least–squares refinement methods based on F^2, using SHELX–97 [1]. An empirical absorption corrections were applied usings SADABS program [2]. The hydrogen atoms were refined isotropically, while the non hydrogen atoms were refined anisotropically. The crystallographic figures have been generated using Diamond 3.0 software [3]. It is worth noting that good quality single crystal data for complex **1** was unsuccessful, despite several attempts to measure this complex. The structure refinement parameters and crystallographic data of complex **1** is listed in **Table S1** and **Table S2**. CCDC−1529126 contains supplementary crystallographic data for this paper. These data can be obtained free of charge from the Cambridge Crystallographic Data Centre via www.ccdc.cam.ac.uk/data_request/ cif.

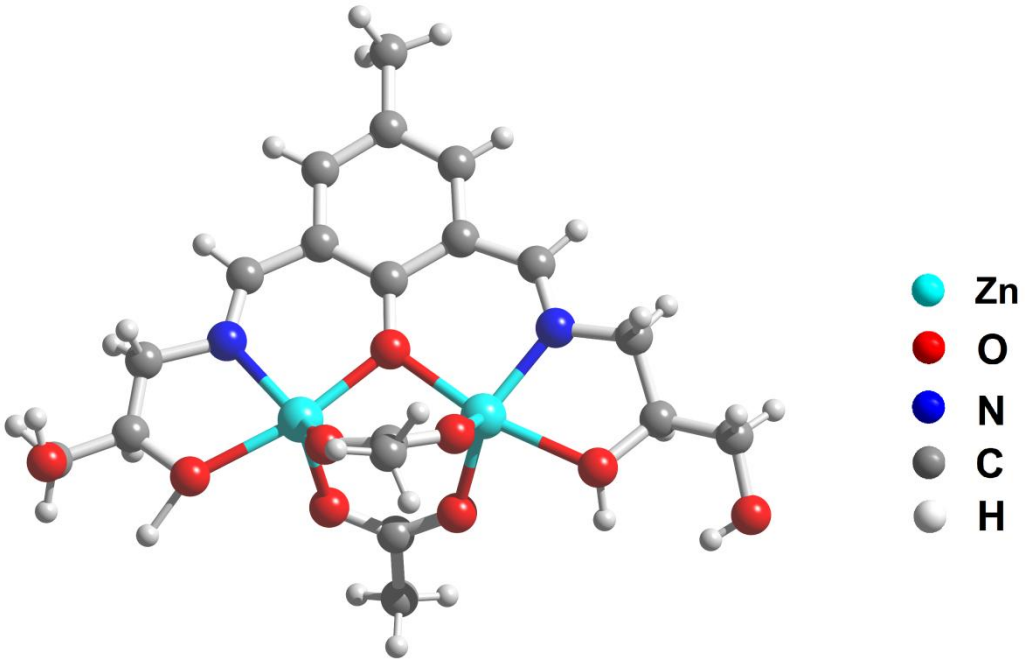

Figure S5. Molecular structure of crystal monocationic Zn^{2+} (complex **1)**. Counter anion was omitted for clarity.

1. Characterization, Structure and Crystallographic Data.

Single Crystal X–ray diffraction: Crystallographic data for complex **1** was collected on a Bruker Nonius Apex II CCD diffractometer with graphite monochromated Mo−K_α radiation (λ = 0.71073 Å) at 296K.

Table S1. Crystal data and structure refinement of complex **1**.

Complex 1	
Chemical formula	C_{20} H_{26} N_3 O_9 S Zn_2
Formula weight	615.28
Temperature/K	296(2)
λ^a/ Å	0.71073
Crystal system	triclinic
Space group	P-1
a (Å)	8.3433(13)
b(Å)	12.2995(18)
c(Å)	15.029(2)
α (°)	85.243(5)
β (°)	84.810(5)
γ (°)	87.894(5)
Z	2
V (Å^3)	1530.0(4)
ρ calc(g/cm^3)	1.336
μ(mm^{-1})	1.680
F(000)	630.0
θ min−max (°)	1.4 to 24.2
Reflns collected	15705
Independent reflns	4826
R(int)	0.0352
S(GOF)	0.950
R1, *wR2*(*I*>2*σ*(I))a	0.2368^b, 0.6462^c
R1, *wR2*(all data)b	0.2431, 0.6685
largest diff peak, hole/e Å^{-3}	11.853 and -1.381

^{a}Graphite monochromator, $^b R_1 = \Sigma(|F_o| - |F_c|)/\Sigma|F_o|$. $^c wR_2 = \{\Sigma[w(|F_o|^2 - |F_c|^2)^2]/\Sigma[w(|F_o|^2)^2]\}^{1/2}$

1. Characterization, Structure and Crystallographic Data.

Table S2. Selected Bond distances (A˚) and angles (°) in the metal coordination spheres of complex **1**.

Table S2. Selected Geometrical Parameters (Distances/Å and Angles/deg).

bond lengths (°)		**bond angle (Å)**	
Zn1 – O4	2.015(13)	O4–Zn1–O6	100.2(5)
Zn1 – O6	1.996(10)	O4–Zn1–O7	98.0(4)
Zn1 – O7	2.002(10)	O4–Zn1–O9	166.9(5)
Zn1 – O9	2.187(13)	O4–Zn1–N1	92.0(5)
Zn1 – N1	1.999(12)	O6–Zn1–O7	109.5(4)
Zn2 – O4	2.047(11)	O6–Zn1–O9	90.0(5)
Zn2 – O5	1.997(11)	O6–Zn1–N1	129.5(6)
Zn2 – O8	1.937(11)	O7–Zn1–O9	86.2(5)
Zn2 – O10	2.227(11)	O7–Zn1–N1	117.0(6)
Zn2 – N2	2.023(15)	O9–Zn1–N1	75.1(5)
		O4–Zn2–O5	98.9(5)
		O4–Zn2–O8	97.3(5)
		O4–Zn2–O10	167.6(5)
		O4–Zn2–N2	90.0(6)
		O5–Zn2–O8	105.2(5)
		O5–Zn2–O10	88.7(4)
		O5–Zn2–N2	134.9(5)
		O8–Zn2–O10	90.1(5)
		O8–Zn2–N2	117.5(5)
		O10–Zn2–N2	77.6(5)

2. Photophysical Characterization.

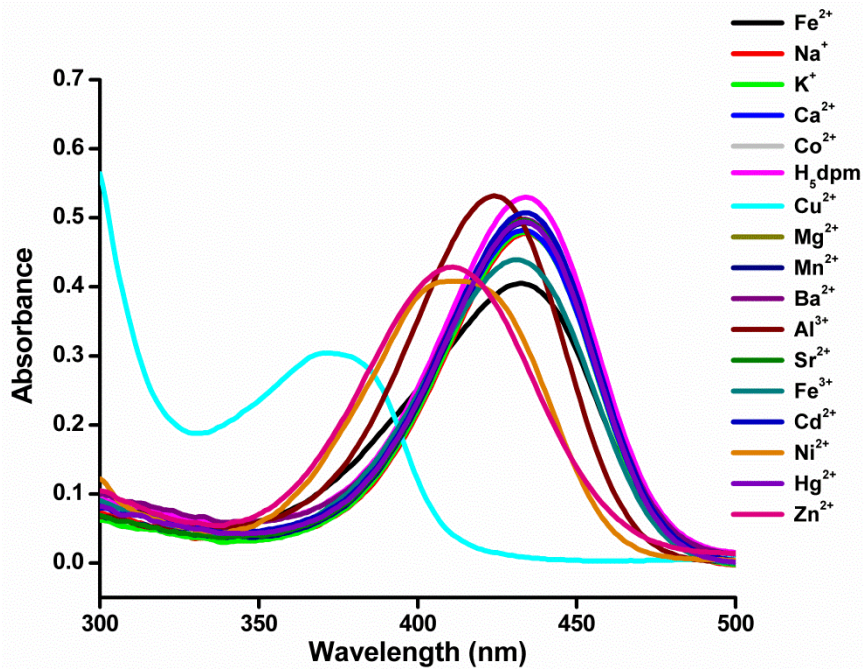

Figure S6. Absorbance spectra of **H_5dpm** (5×10^{-6} M) in Tris-buffer solution in the presence of 10 equivalent of Cu^{2+} and in the presence of 20 equivalent of other metals like Na^{+}, K^{+}, Ca^{2+}, Mg^{2+}, Mn^{2+}, Ba^{2+}, Fe^{2+}, Fe^{3+}, Zn^{2+}, Cd^{2+}, Hg^{2+}, Ni^{2+}, Sr^{2+}, Cu^{2+}, Co^{2+} and Al^{3+}.

2. Photophysical Characterization.

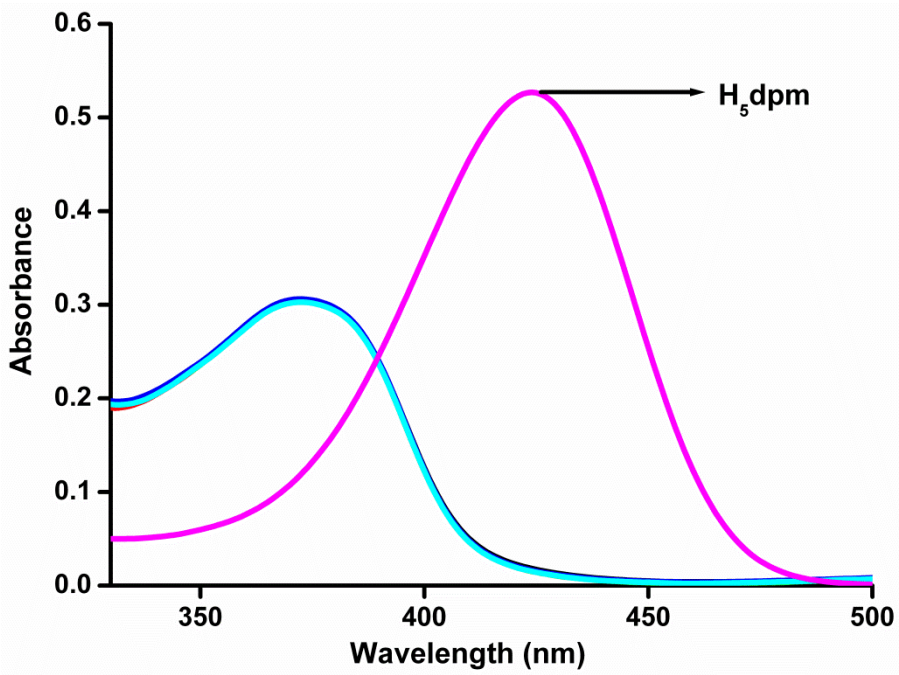

Figure S7. Anion independent absorbance behavior of **H_5dpm** in presence of various Cu^{2+} salts [e.g. $Cu(ClO_4)_2$, $CuCl_2$, $Cu(SO_4)_2$, $Cu(NO_3)_2$ and $Cu(CH_3COO)_2$].

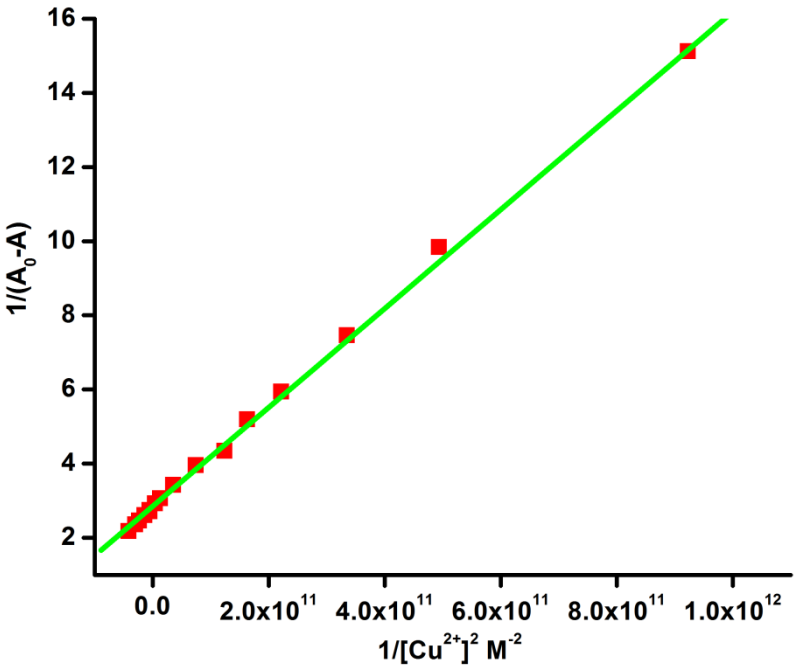

Figure S8. Benesi−Hildebrand plot $1 / (A_0 - A)$ vs. $1/ [Cu^{2+}]^2$ for complexation between **H_5dpm** and Cu^{2+} derived from absorbance titration curve at 434 nm.

2. Photophysical Characterization.

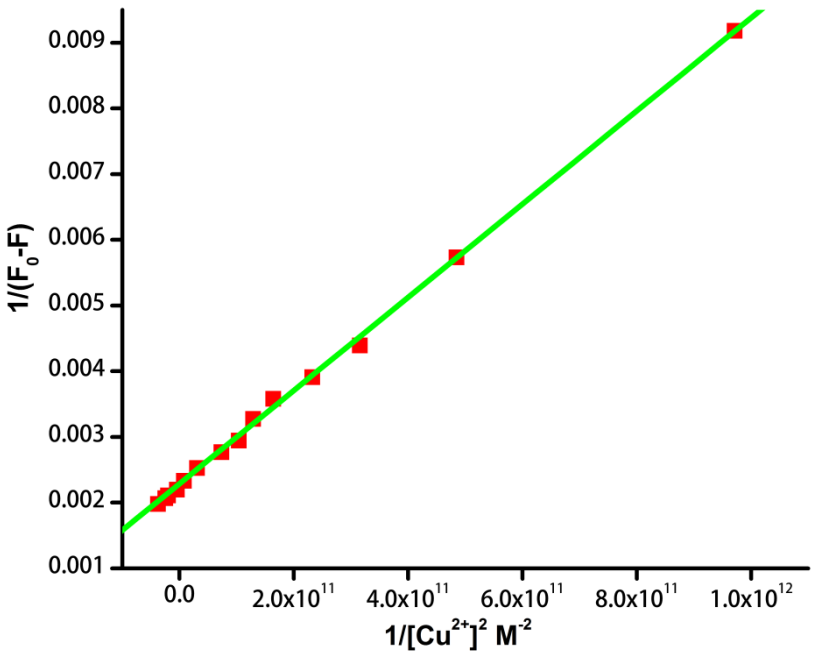

Figure S9. Benesi−Hildebrand plot $1 / (F_0 - F)$ vs. $1/ [Cu^{2+}]^2$ for complexation between **H_5dpm** and Cu^{2+} derived from emission titration curve at 510 nm.

Job′s plot for determination of stoichiometry of Cu^{2+} : **H_5dpm** complex in solution.

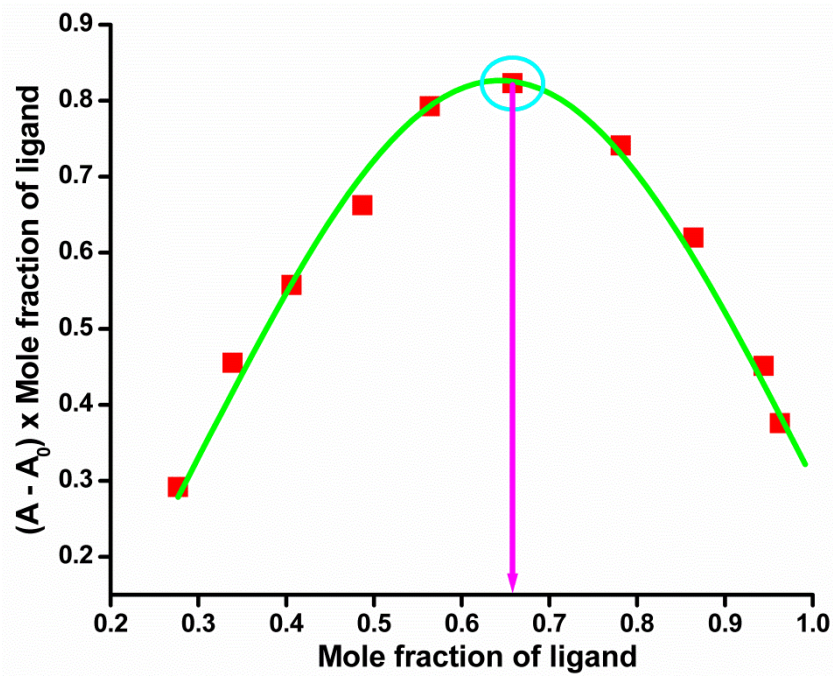

Figure S10. Job′s plot for the identification of **H_5dpm**–Cu^{2+} complex stoichiometry using absorbance values.

2. Photophysical Characterization.

Detection limit calculation in emission spectroscopy.

The limit of detection (LOD) of **H_5dpm**–Cu^{2+} was measured on the basis of fluorescence titration measurement.

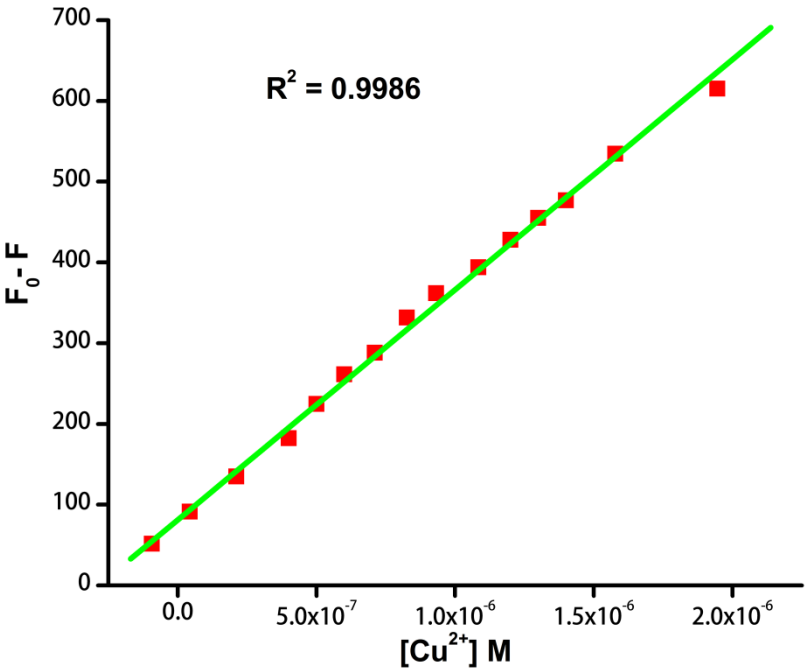

Figure S11. The limit of detection (LOD) of **H_5dpm** for Cu^{2+}: fluorescence responses (λ_{em} = 434 nm) as a function of Cu^{2+} concentration. The solid line represents a linear fit to the experimental data. The detection limit for Cu^{2+} was determined to be 11.2×10^{-9} (M).

2. Photophysical Characterization.

Reversibility studies in UV–vis spectroscopy.

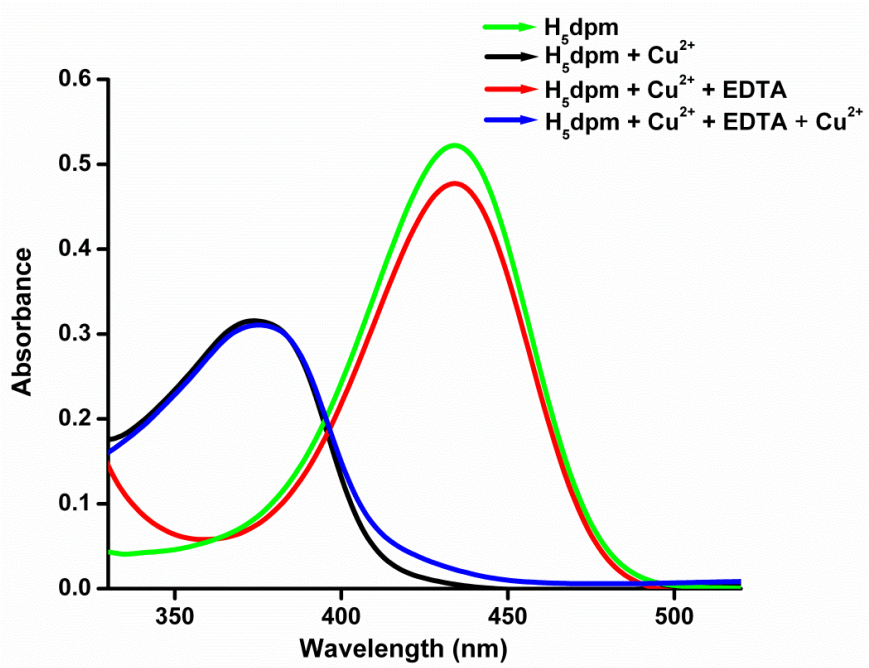

Figure S12. Absorption Spectra of **H_5dpm** in the presence of Cu^{2+} ion followed by addition of EDTA.

Reversibility studies in emission spectroscopy.

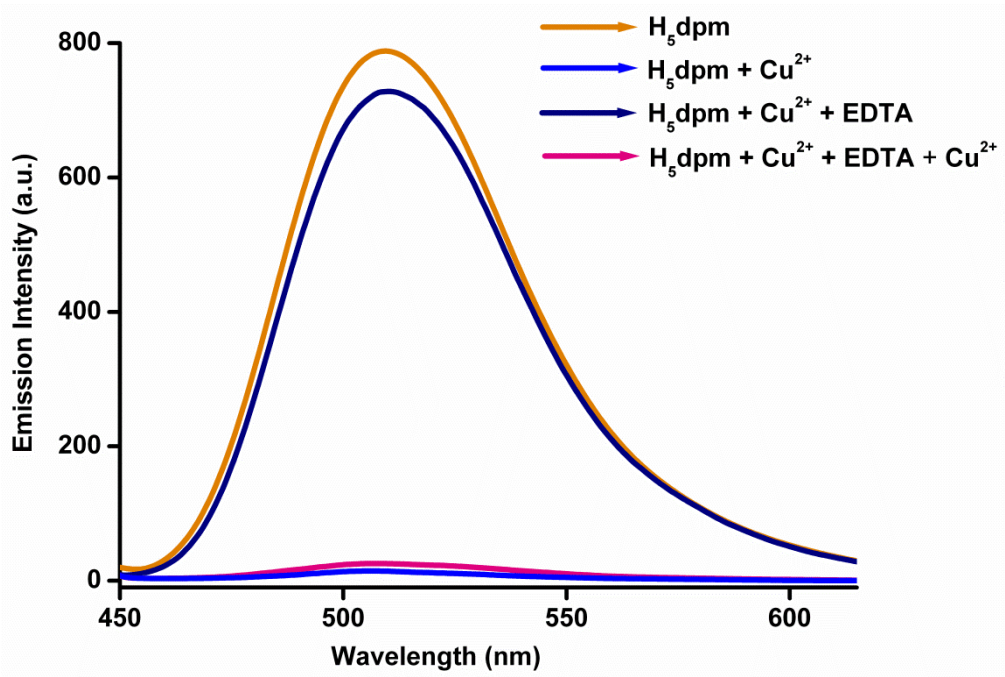

Figure S13. Fluorescence emission spectra of **H_5dpm** in the presence of Cu^{2+} ion followed by addition of EDTA.

2. Photophysical Characterization.

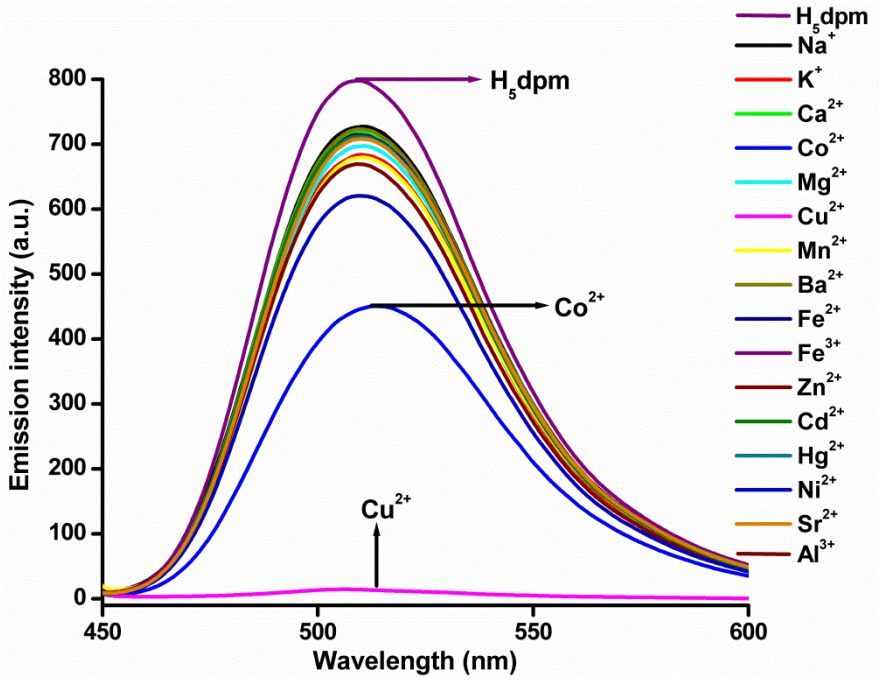

Figure S14. Fluorescence spectra of **H_5dpm** (5×10^{-6} M) in the presence of 50 uM of Cu^{2+} and in the presence of other metals (100 uM) like Na^+, K^+, Ca^{2+}, Mg^{2+}, Mn^{2+}, Ba^{2+}, Fe^{2+}, Fe^{3+}, Zn^{2+}, Cd^{2+}, Hg^{2+}, Ni^{2+}, Sr^{2+}, Cu^{2+}, Co^{2+} and Al^{3+} (λ_{ex}=434 nm, λ_{em}=510 nm, slit: 5nm / 5nm).

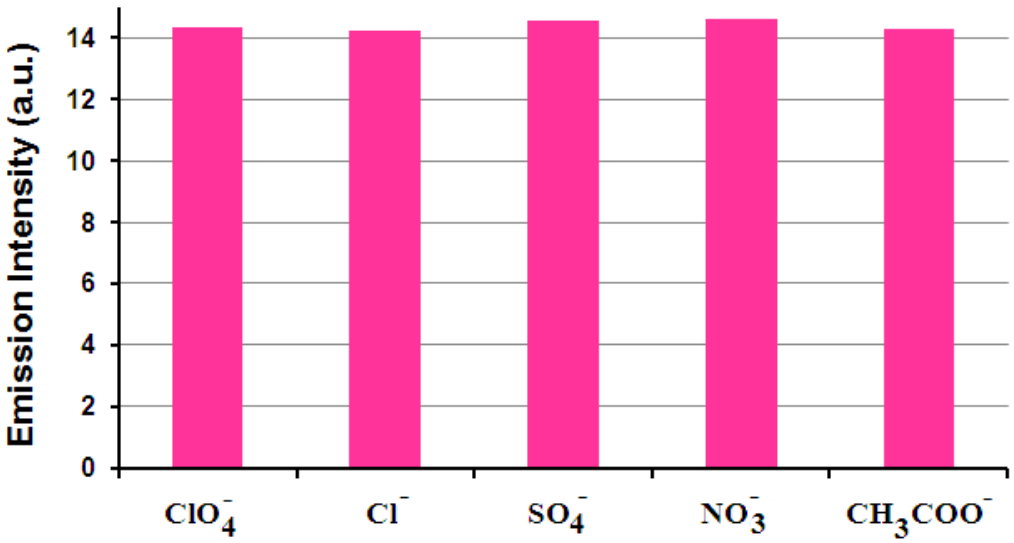

Figure S15. Anion independent Emission intensity of **H_5dpm** in presence of various Cu^{2+} salts [e.g.$Cu(ClO_4)_2$, $CuCl_2$, $Cu(SO_4)_2$, $Cu(NO_3)_2$ and $Cu(CH_3COO)_2$].

2. Photophysical Characterization.

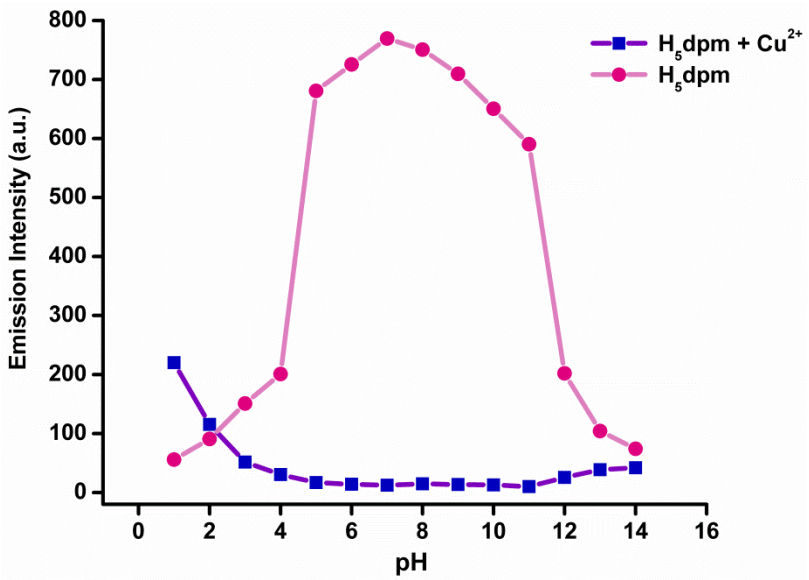

Figure S16. Emission intensity of probe **H_5dpm** (5 μM) in absence and in presence of Cu^{2+} at different pH values in aqueous solution.

Linear solvation energy relationship

E_F (cm^{-1}) = E_0 + Aα + Bβ + Cπ*

E_F (cm^{-1}) = 18974.99805 + 58.9784 α + 118.96533 β + 910.48326 π*

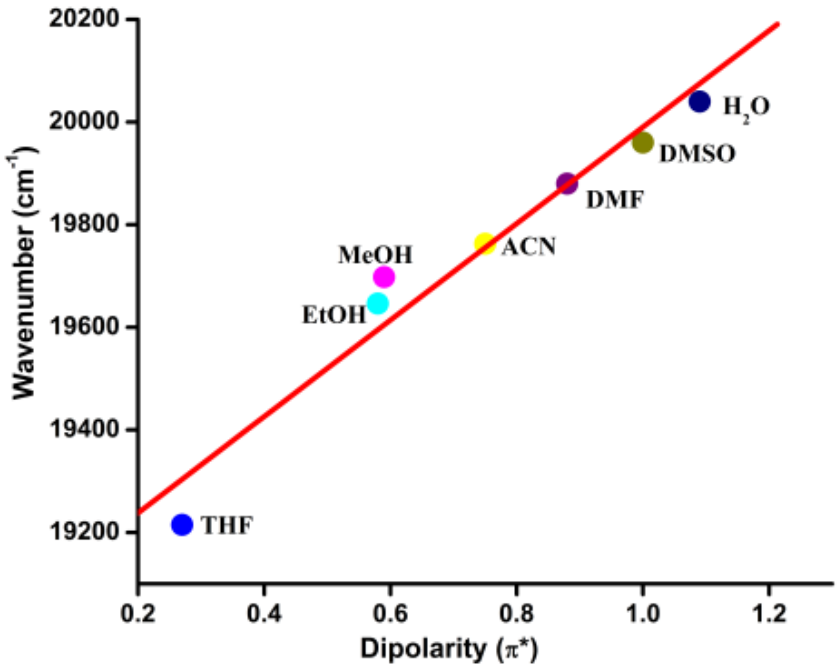

Figure S17. Linear solvation energy relationship plot of wavenumber (cm^{-1}) vs. Dipolarity (π*) for non-specific interaction.

2. Photophysical Characterization.

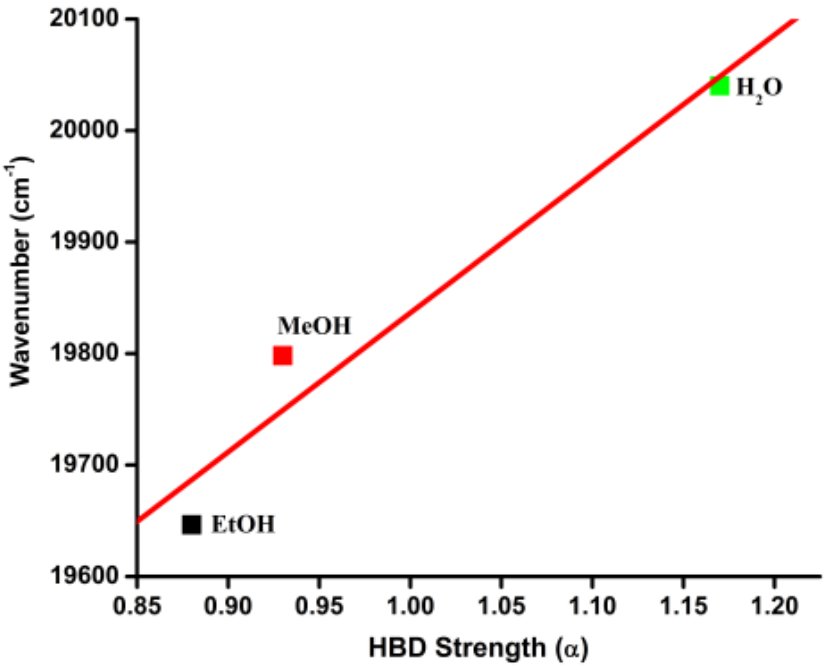

Figure S18. Linear solvation energy relationship plot of wavenumber (cm^{-1}) vs. HBD Strength (α) for specific interaction.

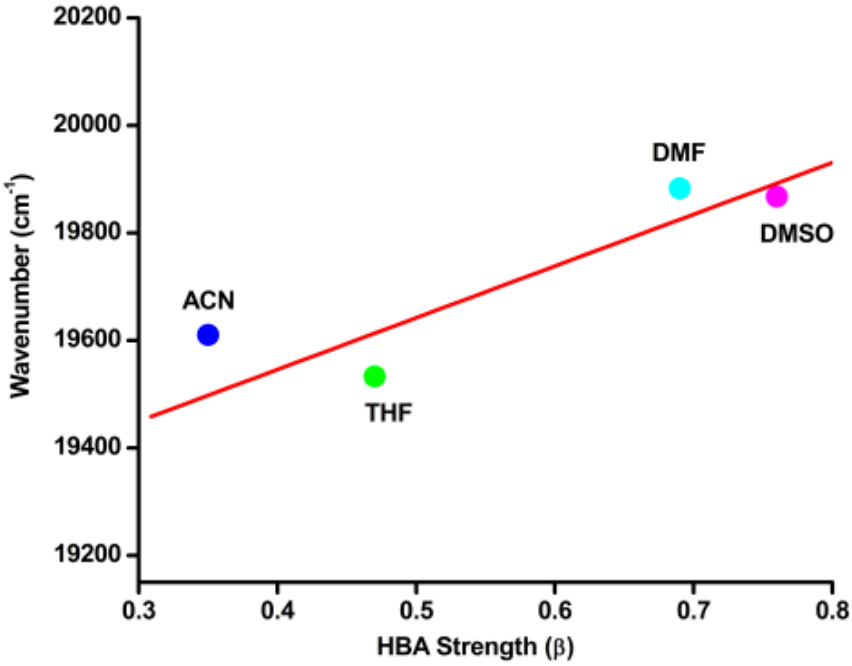

Figure S19. Linear solvation energy relationship plot of wavenumber (cm^{-1}) vs. HBA Strength (β) for specific interaction.

3. Theoretical Data.

In **Figure S20** we show the optimized geometry of complex **2** with a water bridging molecule instead of a MeOH, including some geometric features. It can be observed that it is very similar to the one shown in the main manuscript (see **Fig. 7**)

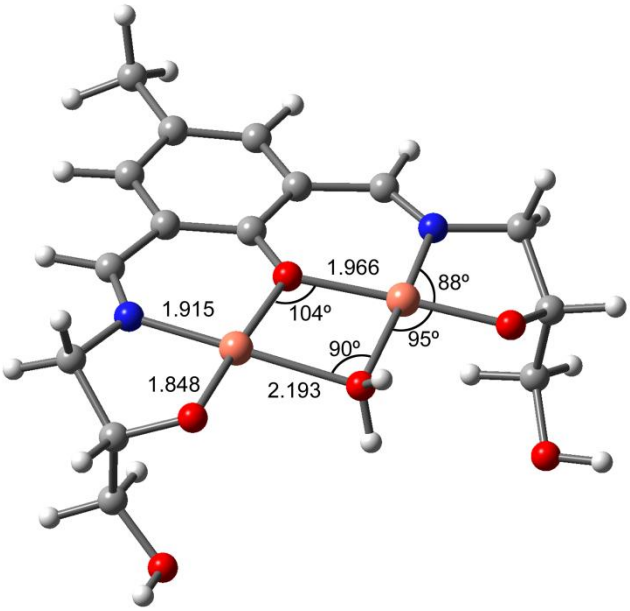

Figure S20. BP86-D3/def2-TZVP optimized structure of $[Cu_2(\mathbf{H_2dpm})H_2O]^+$ complex. Distances are in Å.

In **Figure S21** we show the single occupied molecular orbitals of $[Cu_2(\mathbf{H_2dpm})H_2O]^+$ complex. In the ground state (S_0) of the complex the HOMO and HOMO – 1 are mainly composed by the Cu^{2+} magnetic orbitals (d_{x2-y2}) and some contribution of the atoms of the ligand that are directly bonded to the metal centers (**Figure S21A**, **B**). In fact the spin density plot for the high spin configuration (ferromagnetic coupling) clearly indicates that the spin is located in the Cu metal centers and the atoms directly bonded to them (**Figure S21C**).

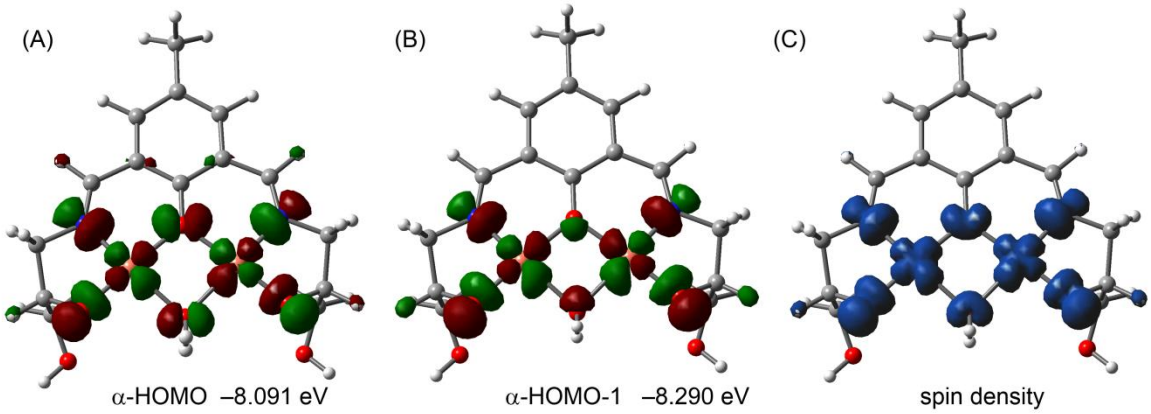

Figure S21. Molecular orbital and spin density plots obtained for complex **2** using H_2O instead of MeOH bridging ligand.

3. Theoretical Data.

Table S3. Selected parameters for the vertical excitation (UV-vis absorptions), electronic excitation energies (eV) and oscillator strengths (*f*), configurations of the low-lying excited states of **H_5dpm**.

Process	Electronic transitions	Composition	Excitation energy	Oscillator strength (f)	Contribution	λ_{exp} (nm)
Absorption	$S_0 \rightarrow S_1$	HOMO → LUMO HOMO–1 → LUMO	2.5516 eV (486 nm)	0.0028	95 % 5 %	-
Absorption	$S_0 \rightarrow S_2$	HOMO → LUMO HOMO–1 → LUMO HOMO–2 → LUMO	2.7962 eV (443 nm)	0.1841	89 % 5 % 5 %	430
H_2O instead of MeOH as solvent						
Process	Electronic transitions	Composition	Excitation energy	Oscillator strength (f)	Contribution	λ_{exp} (nm)
Absorption	$S_0 \rightarrow S_1$	HOMO → LUMO HOMO–1 → LUMO	2.5609 eV (484 nm)	0.0029	95 % 5 %	-
Absorption	$S_0 \rightarrow S_2$	HOMO → LUMO HOMO–1 → LUMO HOMO–2 → LUMO	2.8011 eV (446 nm)	0.1867	89 % 5 % 5 %	430

Table S4. Selected parameters for the vertical excitation (UV-vis absorptions) of complex **2**, electronic excitation energies (eV) and oscillator strengths (*f*), configurations of the low-lying excited states of complex **2**; calculation of the S_0–S_n energy gaps based on optimized ground-state geometries (UV-vis absorption) (MeOH or H_2O used as solvent).

Electronic transitions	Composition	Contribution	Excitation energy	Oscillator strength (*f*)	λ_{exp} (nm)
$S_0 \rightarrow S_{43}$	HOMO–4 → LUMO (alpha) HOMO–13 → LUMO (beta) HOMO–2 → LUMO+2 (beta)	39 % 12% 37%	3.1992 eV (387 nm)	0.0576	375
H_2O instead of MeOH					
Electronic transitions	Composition	Contribution	Excitation energy	Oscillator strength (*f*)	λ_{exp} (nm)
$S_0 \rightarrow S_{43}$	HOMO–4 → LUMO (alpha) HOMO–13 → LUMO (beta) HOMO–2 → LUMO+2 (beta)	39 % 12% 37%	3.2023 eV (387 nm)	0.0580	375

4. Miscellaneous

Chart 1. Comparison of the present probe, **H_5dpm** with some of the recently reported probes for Cu^{2+} encountered in literature.

Probes	Detection limit	Binding constant	Stoichiometric ratio (ligand : Cu^{2+})	Ref.
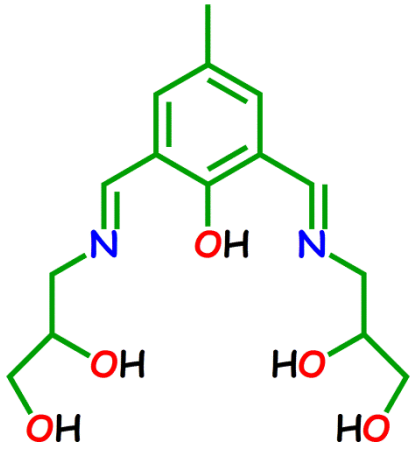	14.3 nM	2.90×10^5 (M^{-1})	1 : 2	In this work
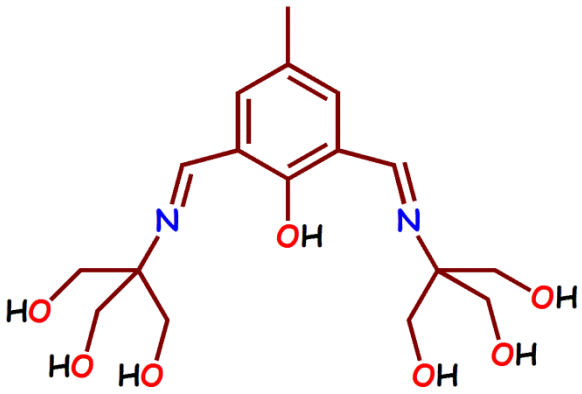	20 ppm	1.0×10^2 (M^{-2}) 4.0×10^4 (M^{-2})	2 : 1 1 : 2	[58]

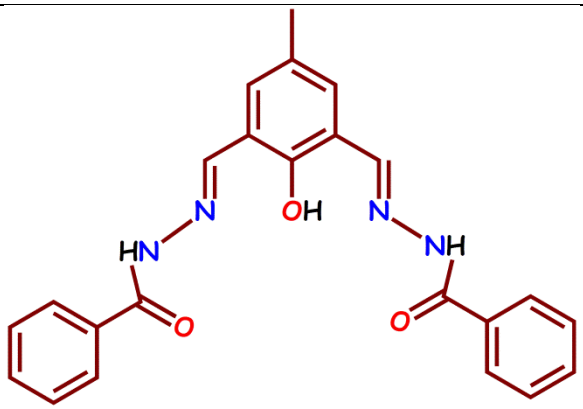	0.272 nM	1.87×10^{6} (M^{-1})	1 : 2	[69]

References

1. G. M. Sheldrick, SHELXL–97, Crystal Structure Refinement Program, University of Göttingen, 1997.

2. G. M. Sheldrick, SADABS, a software for empirical absorption correction, Ver. 2.05; University of Göttingen: Göttingen, Germany, 2002.

3. K. Bradenburg, Diamond, ver. 3.0; Crystal Impact GbR: Bonn (Germany), 2005.